

Carbon Nanotube Based Bearing for Rotational Motions

B. Bourlon, D.C. Glattli* and A. Bachtold†

Laboratoire de Physique de la Matière Condensée de l'Ecole Normale Supérieure, 24 rue Lhomond, 75231 Paris 05, France.

L. Forró

EPFL, CH-1015, Lausanne, Switzerland.

(Dated: November 9, 2018)

We report the fabrication of a nanoelectromechanical system consisting of a plate rotating around a multiwalled nanotube bearing. The motion is possible thanks to the low intershell friction. Indeed, the nanotube has been engineered so that the sliding happens between different shells. The plate rotation is activated electrostatically with stator electrodes. The static friction force is estimated at $\approx 2 \cdot 10^{-15} \text{ N}/\text{Å}^2$.

PACS numbers:

Microfabricated motors have been one of the most studied microelectromechanical systems in the 80s and 90s [1, 2, 3, 4]. Many efforts have been invested in improving performance characteristics such as the rotational speed. It has been shown that the characteristics are mostly limited by the fabrication process through the low reproduction accuracy of the design geometry [4]. For example, microfabrication cannot realize regular enough surfaces at the contact between the rotor and the bearing. These irregularities are important sources of energy loss and reduce considerably the rotational speed.

Multiwalled carbon nanotubes (MWNTs) consist of several nested cylindrical shells. Electron transmission microscopy has shown the high degree of perfection at the atomic level of their structure [5]. Their structural perfection and geometry make MWNTs attractive as elements enabling a rotational motion for nanoelectromechanical systems (NEMS) [6, 7]. Fig. 1a shows the operating principle of such a MWNT element where one or more inner shells can slide with respect to some outer shells.

The utilization of MWNTs as bearings for rotational motion in NEMS has been further motivated by recent experiments that show that the intershell friction can be low in MWNTs [8, 9]. In Ref.[8] the static friction force has been experimentally estimated to be lower than $6 \cdot 10^{-15} \text{ N}/\text{Å}^2$, which gives a very low friction torque due to the thin diameters of the shells. Easy sliding motion between shells has also been predicted theoretically [10, 11, 12]. Interestingly, corrugation against sliding of incommensurate and free of disorder shells is predicted to be extremely small [11].

We report the realization of a NEMS where a metal plate rotates around a MWNT axle. The suspended MWNT is clamped between two anchor pads. The MWNT has been engineered with the electrical-breakdown technique [13, 14, 15], as shown in Fig. 1(a),

to allow access to the inner shells on which is fixed the metal plate. The metal plate is shown to rotate due to surface tension forces of a liquid drop that evaporates on the substrate. The rotational motion can also be activated electrostatically with two stator electrodes. In this way, the plate does not achieve complete rotations but can be positioned in directions lying between the two stator electrodes.

Our rotational NEMSs are fabricated through a four-step process. The MWNTs are synthesized by arc-discharge evaporation and carefully purified [16]. From a dispersion in dichloroethane the nanotubes are dispersed onto a 1000 nm oxidized Si wafer. The nanotubes are imaged with atomic force microscopy (AFM). Thick MWNTs of diameter between 15 and 25 nm are selected because they are mechanically more robust. Their positions are recorded with respect to metallic marks. The nanotubes are then connected with two electrodes using electron beam lithography (Fig. 1(b)). These electrodes will be used both as conducting electrodes and as anchor pads that hold the nanotube bearing. The electrodes, which are 3 μm wide and consist of 10 nm Cr and 60 nm Au, have to be wide and thick enough such that they stay horizontal and suspended when the SiO₂ is etched away at the end of the process.

Fig. 1(c) shows that several outer shells are removed between the electrodes in order to have access to the inner ones. These outer shells are removed with the electrical-breakdown technique [13, 14, 15] that we review briefly in this paragraph. The bias voltage applied on the tube is continuously increased while the current is recorded. When a sharp step in the current is detected the bias is quickly reduced to 0. This sharp step is usually a current reduction of $\sim 20 \mu\text{A}$ which corresponds to the oxidation of the outermost shell. Importantly, the shell is then removed along with most of the tube portion that is not covered by the electrodes. This leaves plenty of room for access to the inner shells.

The electrical-breakdown technique is repeated until several shells are removed to obtain a sliding motion with a lower friction. The sliding will occur through a self-selection process between the shells with the most perfect

*Also at SPEC, CEA Saclay, F-91191 Gif-sur-Yvette, France.

†Electronic address: bachtold@lpmc.ens.fr

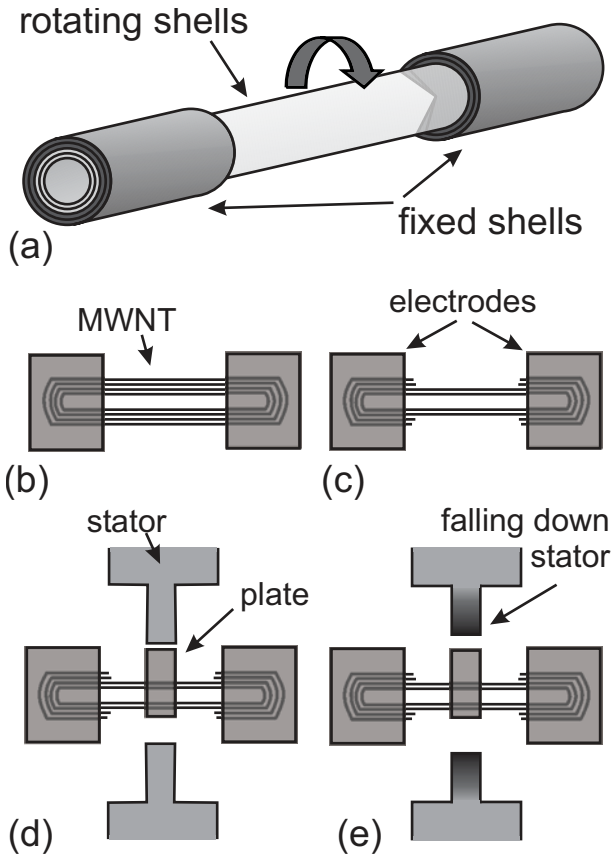


FIG. 1: (a) Inner shells turn inside fixed outer shells. (b) The MWNT is contacted to two conducting anchor pads separated by around $1\ \mu\text{m}$. (c) Several shells are removed between the contacts to gain access to a selected inner shell (d) A plate and two stator electrodes are fabricated. The structures consist of 10nm Cr and 25 nm Au. (e) Etching step with BHF.

surfaces that offer the least resistance to motion. However, we cannot repeat this process until we are left with one or a very few shells as the structure is not robust enough to sustain the drying step at the end of the process. We have found that the samples with inner rotating shells of diameter around 15 nm work well.

Fig. 1(d) shows the structures that are fabricated in a second lithography step. A 500 nm long plate is attached above the rotating inner shells. The plate is asymmetrically positioned with respect to the tube so that the longer section can be electrostatically attracted to one of the two stator electrodes that are fabricated during the same fabrication step. These 200 nm wide electrodes are designed to be narrow so that they will be deposited on the substrate in the etching step making the plate rotation between the two electrodes easier.

The last step of the process consists of etching 500 nm of the SiO_2 with BHF [17]. The wafer is rinsed in DI and in ethanol. It is then dried under nitrogen flow. The ethanol is warmed to just below the boiling point in order to reduce the surface tension. This reduces the risk of the structures breaking down during drying.

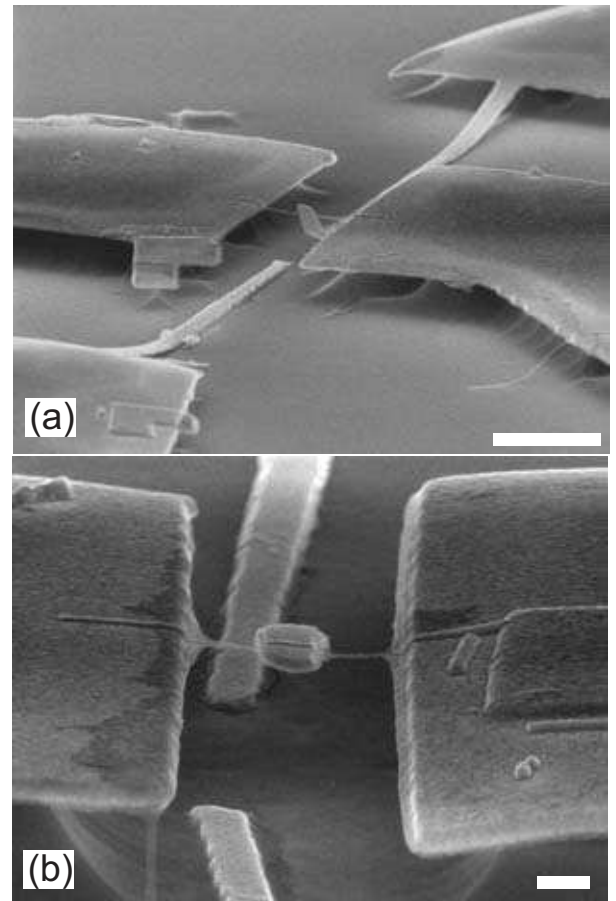


FIG. 2: SEM images of two samples at the end of the fabrication process. (a) Scale bar is of length $1\ \mu\text{m}$. (b) Scale bar is of length 200 nm.

Figure 2 shows two examples of obtained structures at the end of the fabrication process. Interestingly, the plate is not horizontal but has already rotated. The motion has been induced by surface-tension forces of ethanol when drying the sample. Such forces are well known in NEMS fabrication to be important and to deform suspended structures. In contrast, it has been shown that the plate stays horizontal for samples where outer shells of the MWNT are not removed [18]. This indicates that the sliding between the moving and the fixed elements of the NEMS occurs between MWNT shells. Note that the rotation has been observed on most but not all of the samples. In the cases where the plate has not moved, some lithography-resist is observed between the plate and the rest of the structure that may block the motion.

We now show that the plate can be electrostatically driven by stator electrodes. Fig. 3 shows top down images of the device made with a scanning electron microscope (SEM) that has been modified in order to electrically access the different electrodes. In Fig. 3(a) the plate is oriented toward the stator electrode on the right side. A bias voltage V is applied between the plate and the stator electrode on the left side in order to rotate the

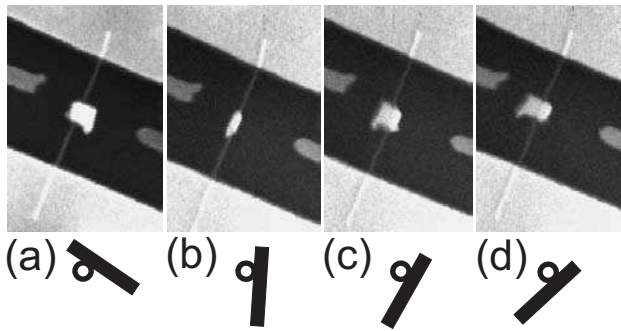


FIG. 3: SEM images recorded when (a) $V = 0$ V (b) $V = 40$ V (c) $V = 49$ V (d) $V = 59$ V. The cross-section schematics below each SEM image represent the rotation of the plate around the MWNT. Both stator electrodes appear less bright than the anchor pads because they are situated at a lower height.

plate in this direction. The motion does not happen at once but occurs in the following manner. V is increased continuously from zero while the other stator electrode and the anchor pads are grounded. The plate stays immobile until 40 V when the plate rotates suddenly to an almost vertical position (Fig. 3(b)). Another angular displacement is observed at 49 V (Fig. 3(c)). The bias has to be increased to 59 V to reach the final position, where the plate faces the biased electrode (Fig. 3(d)).

Importantly, the plate stays in this direction when the bias is turned off. This shows that the rotation is not enabled through the torsion of the tube which would return the plate to the initial position and which occurs for non engineered MWNTs [18]. We note that the plate stays fixed in this direction even if 100 V is applied on the right side electrode. This electrode lies further away from the tube and it is not surprising that the associated electrostatic torque is not enough large to initiate the rotation. Optimization of the design geometry should solve this.

We estimate now the static friction force. Using a finite element method program and the geometry of the plate

and the stator electrode together with $V = 40$ V, we have calculated the electrostatic energy as a function of the plate position. We deduce that the electrostatic couple $\approx 10^{-16}$ Nm. This suggests that the static friction force is $\approx 2 \cdot 10^{-15}$ N/Å² considering that sliding happens on a cylindrical surface that is 1 μ m long and 18 nm in diameter from AFM. This is a low friction value compared with previously reported values, which shows that the electrical breakdown technique is suitable for the fabrication of such NEMSs.

Here we discuss briefly the rotational motion of the plate though a systematic investigation is left open for further work. The plate may block at some specific angles due to variations of the friction between the shells. Friction variation can result from the displacement of some disorder centers situated along the tube or some dangling bonds at the extremities left over from the shell oxidation. Another explanation might be the variation of the capacitance between the plate and the bias electrode. The blockage might then occur when the electrostatic torque becomes lower than the friction torque due to corrugation in the intershell interaction.

After this work was completed, related results were reported in Ref. [19]. A third stator electrode was used in Ref. [19] that has allowed for the complete rotation of the plate around the axle. In contrast to our devices, the electrical-breakdown technique has not been used to engineer the MWNT. The plate has been attached directly on the pristine MWNT. The rotational motion is then obtained by removing one or more outer shells in the region between the plate and the anchors. The removal method is to mechanically fatigue and to shear the outer shells by successive application of large stator voltages.

We wish to acknowledge D. Esteve, P. Joyez, H. Camon and N. Fabre for discussions, B. Placais, J.M. Berroir and C. Delalande for support and P. Morfin for technical assistance. LPMC is CNRS-UMR8551 associated to universities Paris 6 and 7. The research has been supported by the DGA and ACN programs.

-
- [1] W. Trimmer, *Micromechanics and MEMS: Classic and Seminal Papers to 1990* (IEEE Press, New York, 1997).
 - [2] L.S. Fan, Y.C. Tai, R.S. Muller, *Proc. 1988 IEEE Int. Electron Devices Meet., IEEE Electron Devices Soc., San Francisco*, 666 (1988). Reprinted in [1].
 - [3] Y.C. Tai, L.S. Fan, R.S. Muller, *Proc. Micro Electro Mechanical Systems, IEEE Robotics and Automation Council, Salt Lake City*, 666 (1988). Reprinted in [1].
 - [4] M. Mehregany *et al.*, *IEEE Trans. Electron Devices* **39**, 2060 (1992).
 - [5] M.S. Dresselhaus, G.D. Dresselhaus, P. Avouris, *Carbon Nanotubes: Synthesis, Structure, Properties, and Applications* (Springer, Berlin, 2001).
 - [6] M. Roukes, *Phys. World* **14**, 57 (2001).
 - [7] H.G. Craighead, *Science* **290**, 1532 (2000).
 - [8] J. Cummings and A. Zettl, *Science* **289**, 602 (2000).
 - [9] M. F. Yu, B. I. Yakobson, R. S. Ruoff, *J. Phys. Chem. B* **104**, 8764 (2000).
 - [10] J.C. Charlier and J.P. Michenaud, *Phys. Rev. Lett.* **70**, 1858 (1993).
 - [11] A.N. Kolmogorov and V.H. Crespi, *Phys. Rev. Lett.* **85**, 4727 (2000).
 - [12] R. Saito *et al.*, *Chem. Phys. Lett.* **348**, 187 (2001).
 - [13] P. G. Collins, M. S. Arnold, Ph. Avouris, *Science* **292**, 706 (2001).
 - [14] P. G. Collins *et al.*, *Phys. Rev. Lett.* **86**, 3128 (2001).
 - [15] B. Bourlon *et al.*, cond-mat/0305708.
 - [16] J.M. Bonard, *et al.*, *Adv. Mater.* **9**, 827 (1997).
 - [17] J. Nygard and D.H. Cobden, *Appl. Phys. Lett.* **79**, 4216 (2001).

- [18] P.A. Williams, *et al.*, Phys. Rev. Lett. **89**, 255502 (2002). [19] A.M. Fennimore *et al.*, Nature **424**, 408 (2003).